



Numerical and experimental investigation of effective parameters on separation force in bottom-up stereolithography process

F. Yadegari^{1,2}, R. Fesharakifard^{1*}, F. Barazandeh²

¹New Technologies Research Center, Amirkabir University of Technology, Tehran, Iran

²Mechanical Engineering Department, Amirkabir University of Technology, Tehran, Iran

ABSTRACT: Bottom-up stereolithography is included among the additive manufacturing methods, which gives many advantages over top-down stereolithography. The major advantages are related to better fabrication resolution, higher material feed-rate, shorter production time and less material waste. During this process, a separation force is generated as a solidified layer separates from the base of resin container. This force leads to product delamination which in turn stimulates the product failure. An efficient solution to this problem is achieved by studying the interaction force on the specimen contact zone. The approach proposed in this study is based on experimental measurements of the force exerted during the process. Different parameters regarding process characteristics are varied in several tests and a comprehensive analysis is conducted to correspond test condition to the resulting separation force. The significant parameters are process speed, cross-section area, the complexity of geometry and orientation of solidification. For some different cases, the separation force varies between 3 and 36N, and the highest difference between the simulated and experimental results remains beyond 5%. It is observed that higher velocity, larger cross-section area or more part geometry complexity increase the separation force. Another novelty concerns the study of the producing orientation on the separation force. Related experimentation is performed to determine the effect of cross-sectional and geometrical complexity. This article finally gives some preliminary propositions for the part design.

Review History:

Received: May, 30, 2020

Revised: Sep. 06, 2020

Accepted: Oct. 25, 2020

Available Online: Oct. 30, 2020

Keywords:

Bottom-up stereolithography

Separation force

Fracture mechanics

Finite element

3D printing

1- Introduction

Additive manufacturing (AM), widely known as 3D printing, is a new technology that fabricates high complexity components directly from the computer-aided design (CAD) data by adding materials layers by layers. These materials can be plastic, metal or even the human body tissues. Despite the variety of traditional manufacturing methods, producing complex geometries is a challenge that exists, and can lead to changes in design and move away from optimal aspects due to their significant limitations. Using this technology provides some advantages including no need to die making, apply design changes without requiring any additional costs and eliminating tool constraints. All these interesting features seem suitable for the newly appeared applications like personal production, post-modern perspective and complex biological organs printing.

However, despite all the achieved advances and increasing use of this technology, especially during the last decade, some technical challenges persist. Low surface quality, expensive machinery, low reliability and reproducibility, limitations of compatible materials are enumerated as typical deficiencies of additive manufacturing technology [1].

1- 1- Basic concepts

Among a variety of additive manufacturing processes, two ones based on polymerization, including stereolithography and digital light processing (DLP). These optical processing methods use a light-sensitive liquid resin which is solidified by laser beam. They are thereby known as the most important additive manufacturing processes with high precision and surface quality in comparison with the other processes. Because of the close operational principle between these two methods in production of similar models, while the process mechanics is studied, in order to expression ease, the slight difference between solidification light methods is ignored [2]. According to the setup type, DLP method is used in this article. Until now, a few considerable studies are presented for this process and the referred surveys are majorly founded on empirical work and practical try and test approaches. In the theoretical issues, the knowledge about physical and chemical changes during the light radiation is very limited, and the variety of using materials aggravates the problem situation [3,4].

The mechanism of material feeding in the stereolithography process is considered a very effective factor in reliability and power consumption and is executed in two general ways: free-surface (top-down) and constrain-surface (bottom-up). In the constrain-surface method, the setup platform moves up

*Corresponding author's email: fesharaki@aut.ac.ir



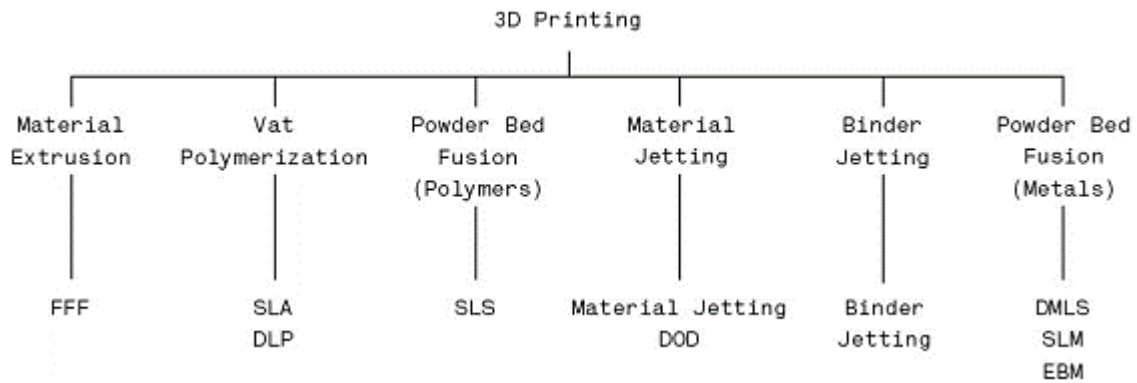


Fig. 1. Classification of 3D printing and the processes based on polymerization [2].

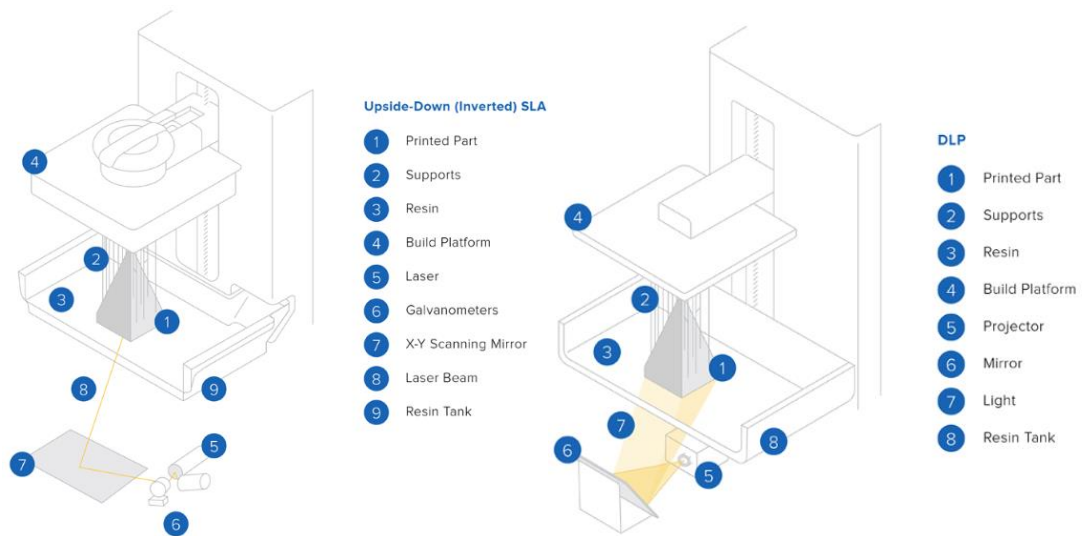


Fig. 2. Schematic view of digital light processing (right) and stereolithography (left) methods [18].

to a specified amount of d , after finishing the solidification of a layer, afterward goes down for $d-l$. The value of l expresses thickness of layer. This procedure achieves better vertical resolution because the desired thickness of the fabrication layer is always between the two surfaces, the bottom of the tank and the moving platform, so could precisely be controlled [5]. Also in this method, despite the lower amount of material, the feeding rate will be better. On the other hand, there is no radiation of light beams in the air which results in reduction of energy level [6]. In addition, because the need to sweeping the resin for the surface smoothness in each step is eliminated, no factor prevents the high speed production using this method.

Despite the described prominent advantages, the parts produced by the constrain-surface method prominently faces an important challenge that concerns the separation of each layer after solidification from the resin tank base. The large interaction forces arising at this stage of the process, cause the part damage. The most important consequence of such event

is the phenomenon of delamination, which means that the layers are not properly adhered together. This phenomenon fails the part either during the process or then while exerting external loads.

1- 2- Literature review

As shown in Fig. 3, in the constrain-surface method, the producing layer is situated between the previously solidified layer and a polydimethylsiloxane (PDMS) silicone film surface. This surface acts as a coating to reduce the separation force applied on the bottom of the tank [6] and confines its effect. When the platform moves upwards to take the position for next layer, the silicone film supports some elastic deformation and separates the surrounding boundaries as for the starting position.

In the following, a review of investigations done to reduce or eliminate the separation force is given. In general, the solutions provided in this context are composed of three general categories: comprising composite material for

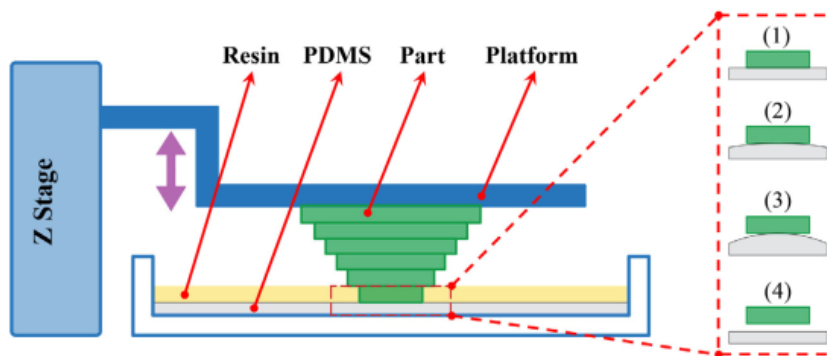


Fig. 3. The separation steps of the producing layer and the resin tank during the process [6].

coating, chemical solution and mechanical one.

The first option concerns covering the tank floor with suitable materials that participates in removing the part from the platform and reducing the generated separation force. The most common materials for these coatings are Teflon and silicon films. For example, Denken[®] and EnvisionTek[®] commercial machines use the Teflon coating. However, the separation force remains significant. Another mechanism called E-DARTS developed by Autostrade[®] uses silicone film on the bottom of the tank [6,7]. One important limitation of this method is the limited life of coating. Since after several stages of printing, this coating loses transparency, subsequently its performance falls down. The related life cycle depends on the amount of separation force. So that by increasing this force, the life cycle of the coating will be significantly reduced.

Another method uses the gas permeability of the material applied to the bottom of the tank. By choosing a proper geometry of the area, the contact surface of the gas-permeable layer increases with air and a non-reactive multi-micron thick layer forms at the resin solidification side. Thereby the separation force is reduced to about 60% [7]. Based on this mechanism, Carbon3D[®] corporation has introduced CLIP technology that can print parts at high speeds. This result is achievable by the dramatic decrease in the separation force [8]. This method is however limited since it merely permits the production of grid-patterned parts, where the cross-sectional area in each layer is negligible. This means that the production of continuous cross-section parts with significant area remains a serious challenge.

In the last approach, the system is completed by some linear or rotational mechanical motions. This method works by eliminating the contact between the resin vat and the part after producing each layer with the help of a linear motion in the horizontal direction or a rotation of the tank perpendicularly to the part-producing direction[9]. Obviously, each linear or

rotational motion is an additional step in the fabrication for each layer. The first negative result is reducing the production rate. This method may also not completely eliminate the effect of the separation force, because it is suitable only if the part is close enough to the rotated side. Therefore, the mechanism efficiency in this process could not be evaluated [5].

In addition to the operational approaches that have previously been implemented, some analytical studies were carried out to investigate the effect of different parameters on the separation force within both experimental and simulation results. The majority of these studies were limited to simulation and the others used each time one type of a specific resin [10]. In this article, a new type of DSM Somos[®] series resin is used and besides the experimental tests for measuring the force, the process is simulated by finite element analysis. The interesting point of this study concerns the force measurement method performed through a direct mechanism providing more precision. The other novelty is related to evaluating a part-producing orientation. Once the simulation and experimental results are given and compared against each other, a discussion is given in the last section to validate the results.

2- Separation Force Parameters

2- 1- Cross-section geometry and velocity

As stated earlier, in the constrain-surface mechanism of the stereolithography method, when the light is irradiated at each step, the platform moves upwards in z direction and separates the layer from the bottom of the tank. In the meantime, the liquid resin fills the gap created by the separation process with the help of existing suction pressure. As shown in Fig. 4, the separation force will arise at this stage. In this figure, the part is pulling up with the velocity V . The parameters A and h , respectively denotes the printed cross-sectional area and the distance between this surface and the bounded surface (tank floor) [12].

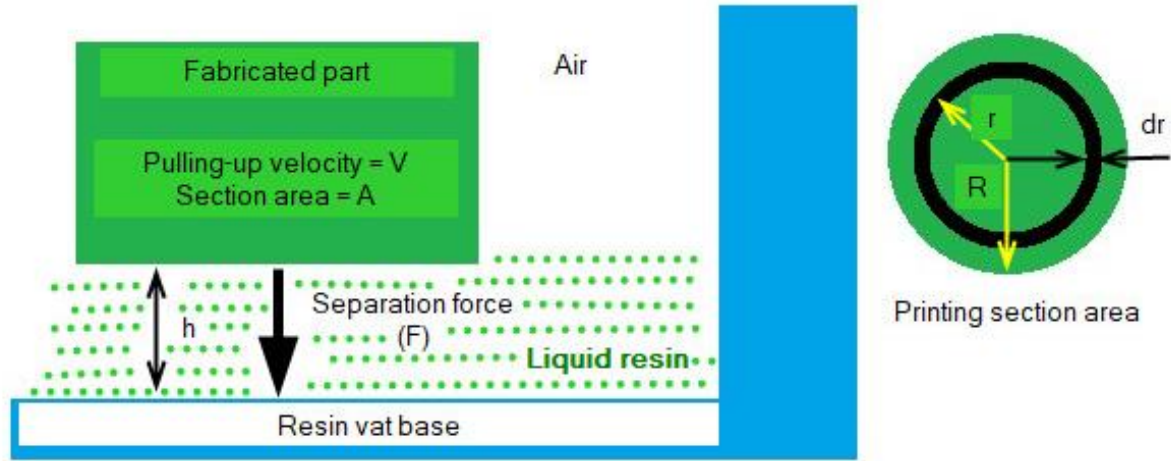


Fig. 4. Schematic view of the separation force in a cylindrical part.

In order to analyze this issue, simple modeling has been done to achieve and investigate the governing relationships. First, a model of a cylinder with radius R in cross-section is examined and the resin viscosity is assumed constant. Based on the Navier-Stokes equations, the flow rate of the fluid resin is expressed by the following equation [11];

$$u = \frac{1}{2\mu} \frac{dP}{dr} (Z^2 - Z.h) \quad (1)$$

Then, based on the mass conservation law, the relationship between the platform speed in the Z direction and the resin flow rate will be as follows;

$$V \cdot \pi \cdot r^2 = 2 \cdot \pi \cdot r \int_0^h u dz \quad (2)$$

By substituting Eq.(1) in Eq. (2), the following equation will be obtained:

$$V \cdot \mu \cdot r = \int_0^h \frac{\partial P}{\partial r} \cdot (Z^2 - Z.h) dZ \quad (3)$$

Integrating both sides in the above relationship gives:

$$P = -\frac{3\mu V}{h^3} \cdot r^2 + C \quad (4)$$

Then by applying the boundary conditions $r = R$ and $P = 0$, the pressure will be calculated as follows:

$$P = -\frac{3\mu V}{h^3} \cdot r^2 + \frac{3\mu V}{h^3} \cdot R^2 \quad (5)$$

At last, by integrating the pressure on the area, the following equation will be obtained for the separation force:

$$F = \int_0^R 2\pi r P dr = \frac{3\pi \cdot \mu V}{2 \cdot h^3} \cdot R^4 \quad (6)$$

This equation shows that the separation force F is nonlinear with R and h and has a linear relationship with velocity V [11]. As it can be seen, the separation force is related to the fourth power of the radius of the part being processed. This means that doubling the size of the cross-sectional area leads to 16 times increase in the separation force and this huge force will easily break the production block. This has been the main cause of the many solutions proposed to reduce the separation force. In fluid science, this force is called Stephen's adhesion and states that, regardless of the materials involved in the process, there will always be a bonding force between the two flat surfaces involved in a fluid environment [12].

According to the above model, it is found that the variables affecting the separation force so far include the viscosity of the material consumed, the amount of oxygen-inhibition layer thickness, the z -velocity and the cross-section geometry. Among these, the speed variable has a good controllability and is more precisely adjustable. The variable h is related to

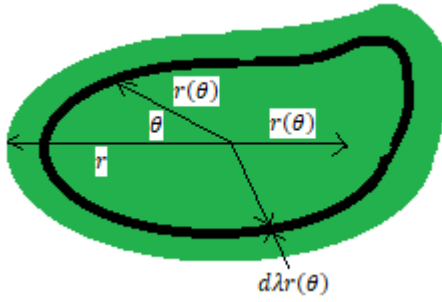


Fig. 5. Considering the print section as an irregular geometry

the oxygen permeability of the coating used at the surface and by making changes to this level, it can be controlled. But the variables of resin viscosity and geometry of the printed cross-section will be determined according to the expected use and end product requirements. Therefore, it can be said that the two variables of velocity and distance have the potential to play a great role in preventing the creation of large separation forces.

In order to generalize the recent relations and apply them to different and more complex geometries, the following model can be used. Similar to above, the fluid velocity equation can be expressed as follows [11];

$$u = \frac{1}{2\mu} \frac{dP}{d\lambda r(\theta)} (Z^2 - Z.h) \tag{7}$$

In this equation, r represents the radius in a certain angle and θ the angle, the coefficient λ remains between zero and one, and h is the distance between the underside of the processed part and the constrain surface of the process. According to the law of mass conservation, it can be written:

$$\lambda^2 . V . A = \lambda . L . \int_0^h u dz \tag{8}$$

where A represents the area of the cross-sectional area and L represents the perimeter around this surface.

$$A = \int_0^{2\pi} \frac{1}{2} r(\theta)^2 d\theta; L = \int_0^{2\pi} \theta . r(\theta) d\theta \tag{9}$$

By substituting the first equation in the second one, the following equations will be obtained;

$$2 . \lambda . \mu . V . A = L . \int_0^h \frac{dP}{d\lambda r(\theta)} . (Z^2 - Z.h) dZ \tag{10}$$

$$P = \frac{12 . \mu . V}{h^3} \frac{A}{L} . \lambda^2 . r(\theta) + C \tag{11}$$

Here, by applying boundary conditions of $P(\lambda = 1) = 0$, the values of pressure and separation force will be expressed by the following equations:

$$P = \frac{12 . \mu . V}{h^3} \frac{A}{L} . r(\theta) (1 - \lambda^2) \tag{12}$$

$$F = \frac{8 . \mu . V}{h^3} \frac{A}{L} . \int_0^{2\pi} r(\theta) d\theta \tag{13}$$

The last two equations show that during printing a solid form, the separation force will be influenced by the combination of the variables of viscosity, velocity, distance h and cross-section geometry. For irregular geometries, the effect of the printed section geometry can be modeled by A/L ratio. Therefore, if other parameters are assumed to be constant, in a specified printing cross-sectional area, a section with a smaller perimeter, will experience greater force and subsequently greater separation stress and this will cause the component's failure. In this case, it can be said that for an existing resin model, lower velocity and a smaller h distance is more suitable for intersections with a smaller perimeter [11].

2- 2- Part Weight

This parameter comprises the total weight of the printed part and the force required to separate the part from the bottom of the resin tank. By printing and depositing each layer, the weight of the piece will increase and affect the amount of calculated separation force. Therefore, after measuring and recording the amount of force in an arbitrary n^{th} layer of the process, the weight of the part should be subtracted from the measured force.

2- 3- Resin temperature and viscosity

In the top-down method, the viscosity of the resin might not necessarily be greater than a limit. In other words, its viscosity should be low enough for the system to work properly, i.e. the resin flows smoothly to the surface. This study demonstrates this effect and indicates a proper flow displacement in the platform. On the other hand, it shows how the viscosity of the resin is effective on the produced part characteristics. Because a layer being processed is confined between the bottom of the tank and the previous layer, great

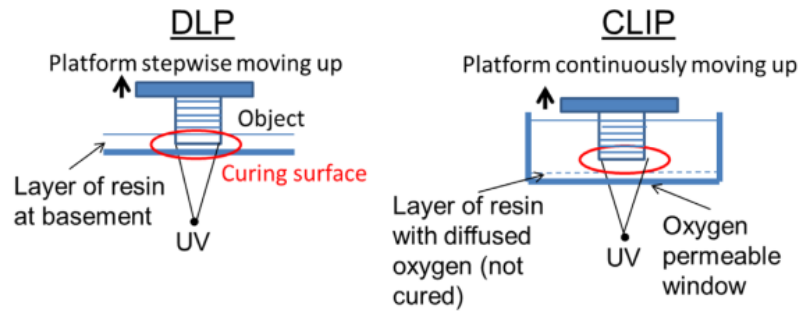


Fig. 6. Decrease of adhesion force by inactivating area due to the permeability of the tank floor layer [19].

viscosity intends to cause low deformations in the layer and eventually the part.

As the temperature increases, the viscosity of the resin decreases. As the separation force is greater for high viscosity resins, these two properties are pertinent considering their effect on the separation force. Thus the expected performance of the end part is majorly determined by their values. However, a direct relation to predicting the direct effect of these parameters on mechanical properties of the processed part is not evident because of the other influencing parameters [7,12].

2- 4- Buoyancy forces

The relative weight of the platform decreases when it touches the resin surface. As the platform immerses in the resin, more pressure is applied to its surface. In fact, this gap between the platform and the tank surfaces (h) is a affective parameter for the separation force. This indicates that as the platform deeps further and h decreases, the separation force will in turn increase. Stephen's adhesion equation also confirms this effect and predicts that the distance h has a great influence on the amount of oxygen penetrating into the silicon coating at the bottom of the tank [12].

2- 5- Radiation duration and layer thickness

At the beginning of the process to ensure that the part adheres to the construction platform, the irradiation time of the first layers is considered more than usual. But in the next layers, the desirable goal is to reduce this radiation time to minimize adhesion and consequently the possibility of part failure. On the other hand, with more radiation time, the solidification thickness will increase. Therefore, it seems that increasing the irradiation time as well as increasing the thickness of the layers, which is in turn stimulated by increasing the irradiation time, will both increase the separation force.

2- 6- Oxygen inhibition layer thickness

The chemical base of the 3D printing method is related to radical polymerization of acrylate monomers. To initiate the polymerization process of a resin, it should first consume and then solve all the present dissolved oxygen in the process [12]. In fact, the oxygen present in this area is a deterrent for initiating the reaction and solidifying the resin, and simultaneously can be used to reduce the amount of separation force. Since DLP printers use silicone or Teflon coatings on the bottom of their tanks, acting as coatings that permeable layers to the gas, they use this oxygen diffusion property as a mechanism for separating the solid layer from the coating. At the point of contact between the resin and the coating, there is a thin layer of unreacted and oxygen saturated monomer, with a thickness between 1 to 50 microns for silicon-based printers [7].

At the side of radiation window, there is a thin layer of unreacted monomer that slowly shrinks and disappears. This thin layer allows significantly reduces the separation force. This mechanism is actually the basis of high-speed printing methods, which also have significant costs compared to conventional ones. With respect to the parameters mentioned above, the relation of the separation force with the main process parameters could be illustrated as follows. It is almost possible to say that most of the solutions presented are aimed to reduce the effect of each factor in the following equation.

$$\text{Force} = \text{Viscosity} \times \text{Area} \times \text{Speed} / \text{Gap} \quad (14)$$

3- Force Measurement

In the next section, the parameters that are as inputs for the simulation phase will be calculated and in the first

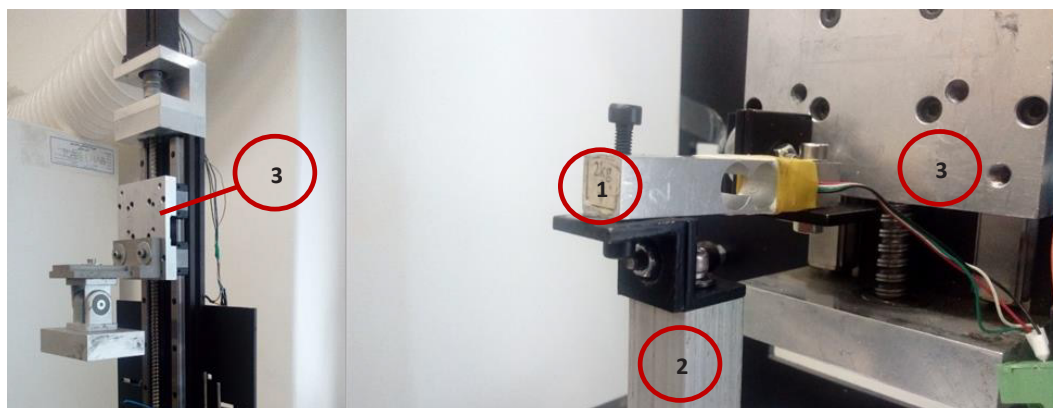


Fig. 7. Locating and installing the load cell on the setup. 1: Load cell, 2: Build Platform and 3: Motion System

step, the force measurement is described. For this purpose, a setup is prepared as shown in Fig. 7. Then the other needed parameters are obtained by using the measured force based on a fracture mechanics concept of cohesive zone model or CZM.

3- 1- Experimental setup

In this experiment, the traction forces have been measured and recorded in several different tests. The operation is carried out on a set of load cell assembly and electronic boards after verification. Then the setup is mounted on a Kavosh[®]-Laser DLP machine. Due to the geometry, material and capacity of the load cell, a different and lighter structure is proposed to reduce the maximum weight of the platform structure and subsequently reduce measurement errors. This design enables the 3D printing process to be monitored online with a proper implementation based on the non-destructive evaluation.

The transparent plexi-glass sheet is used to compose the resin tank. Plexi-glass is a very transparent plastic type of polycarbonate polymer. This material is highly resistant in comparison to glass and resists well against UV while conserving its transparency. The polished surface and light permeability make it useful in the manufacturing of resin tanks of DLP machines. In the presented tank, the cross-section of the resin holder varies between 42 and 55 mm and a layer of 2 mm thick silicon film covers the bottom.

3- 2- Load cell calibration

Four different weights are used to evaluate the load cell precision: 1177.5, 100, 50 and 20 g, respectively. Initially, all weights are placed on the load cell for 3 seconds. Then, in three steps, weights of 20 g, 50 g and 100 g, are removed from the load cell respectively. In each of these steps, the obtained weight values are recorded, and this operation is repeated 5 times. The maximum load cell error is about 0.004 N, which indicates enough precision for use in this study. Next, to calibrate the dead load effect on the load cell resulting from the weight of approximately 145 g of platform

body, the necessary adjustments are performed by using the precision weights.








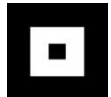




3- 3- Experiment procedure

In this experiment, six different patterns with specific effect studying purposes are used. The six patterns consist of three squared sections with different areas, in order to study the cross-section area and three squared sections with interior holes to study the geometry complexity. The experiment is also performed at different speeds to investigate the speed of the separation force. An illustration of each of these patterns, along with the necessary process and dimension specifications, is presented in Table 1.

After specifying the desired radiation patterns and modeling them in 3D using CATIA software, and extracting in STL format, each model is divided into 30 layers of 100 microns using NetFabb Studio basic Version 4.9 and Slicee software, and then sent to the controller and optical system of machine.

In the manufacturing process, the first layers usually require a longer irradiation time than the next layers to ensure a properly bonded part to the surface of the production platform. This period for the first layers is approximately 10 times greater than the next ones. So the necessary time for several trial and error tests is given to the machine controller. In this experiment, after finishing the ninth layer, the separation force is measured in the tenth layer. As mentioned earlier, each layer has a thickness of 100 microns, so the height of the solid part is 1 mm when measuring the separation force. For this reason, the tenth layer is considered to measure the force, and according to several tests of the process, it is observed that as the layers are processed, the probability of part failure is increased due to the large separation forces and which are no more precisely measurable. On the other hand, there can no more be a proper analysis based on the behavior of the first layers. Because these layers are produced in conditions other than the others. One of the reasons is the longer exposure time to the light, which increases the force for this layer.

Table 1. Geometric Properties of Printed Patterns.

Dedicated Design Name	CAD Model	Cross section pattern	Dimensions (mm)	Area (mm)	Description
A2			10 x 10	100	
A3			15 x 15	225	This model is considered as the benchmark model.
A4			20 x 20	400	
P1			15.81 x 15.81	225	Holes dimension 5 x 5 (mm)
P4			18 x 18	225	Holes dimension 5 x 5 (mm)
P9			19.2 x 19.2	225	Holes dimension 4 x 4 (mm)
V1/V2/V3/V4/V5	The pattern used in speed tests was the A3 pattern				

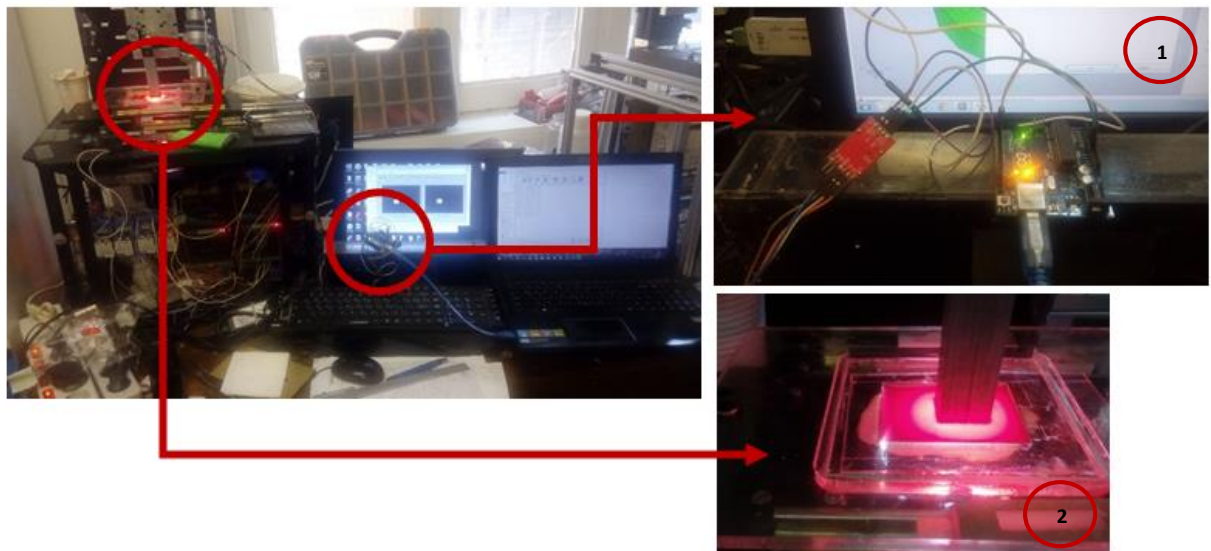


Fig. 8. Setup of experimental measurement of separation force. (1) Arduino® board and its amplifier, (2) Resin vat during the process

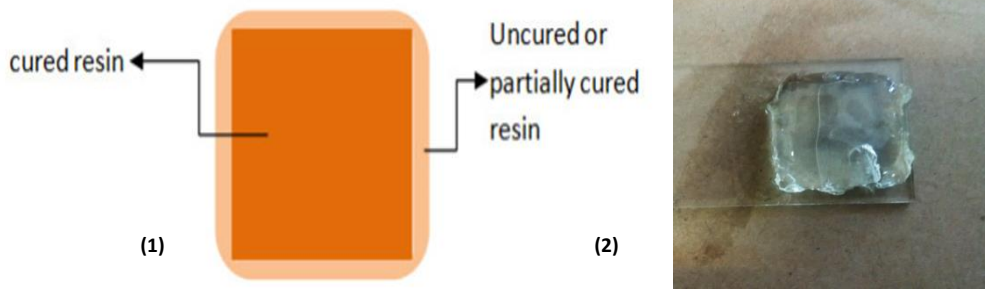


Fig. 9. Partial solidification of transparent resin around the pattern due to light scattering. (1) Schematic view (2) Processed part.

Due to the transparency of the used resin, the first challenge that emerged during the experiment is the light scattering in different directions around the pattern which results in partial solidification of the resin and accuracy reduction and pattern error. When the experiments are run to investigate the effect of cross-section geometry on separation force, this problem will lead to major errors and obliges an appropriate solution. To this end, by adding some red color pigments, the scattering of light is prevented and the parts are printed with very good dimensional accuracy.

4- Modeling

4- 1- Cohesive zone model

Linear elastic fracture mechanics provides a suitable tool for fracture analysis of cracked structures. In this domain, the nonlinear behavior of the crack tip is ignored and it is obvious that this approach does not predict all structural behavior like soft metallic and non-metallic materials such as polymers. In the process of breakthroughs in fracture mechanics.

The separation process in the present work can be viewed as a delamination process in laminated composite materials. From this purview, the separation of the cured part from the PDMS film will be modeled here by relying on the mechanics-based concept of the delamination process [14]. There exist several methods to model the delamination process in the fracture mechanics literature. Virtual crack closure technique (VCCT) [20] and cohesive zone model (CZM) [21] are among the most popular methods. While the VCCT has been successfully used in simulation of crack delamination process, it has not been broadly implemented in most of the existing FE software because of certain disadvantages. For example, this method cannot predict delamination initiation and can only predict propagation of existing crack. A pre-existing crack with a sharp and neat tip, therefore, would be required for crack initiation [22]. Such information is not applicable and cannot be defined in the present work. Comparing to VCCT, a major advantage of the CZM is that it can predict both the initiation and propagation of delamination without the requirement for a pre-existing crack [22]. It is also applicable

to complex structures subjected to complex loading states. The CZM has been extensively used for delamination and debonding processes.

CZM model describes the adhesive region of the material failure regardless of material structure, and the model parameters are dependent only on the material and not on the geometry of the cracked part. This model is extended from simple examples to the structure with complex geometries. In this model, surface separation occurs within an adhesive damage area. When the damage exceeds a specified permissible level, an active tensile stress interaction occurs between the adhesive surfaces. The law of traction-separation describes this interaction. According to this law, no damage occurs in the adhesive area prior to applying a load. As seen in Fig. 10, when a damaged element is completely separated, there is no more force between the adhesive surfaces.

As mentioned, the separation relation is defined as follows:

$$\delta = u^{TOP} - u^{BOTTOM} = \text{Interfacial separation} \quad (15)$$

In this equation, δ denotes the amount of the generated separation and u represents the displacement values for each of the two involved layers. There are several ways to express material behaviors in the adhesive area, such as bilinear, exponential, trapezoidal and trilinear ones. These diverse models provide a wide range of modeling material behaviors, including nonlinear behavior that cannot be modeled by linear elastic fracture mechanics.

The behavior of the adhesive region in each of the states has its own complexities to be specified. While being simply impossible to directly measure the cohesive area parameters, there is almost no way to implement an empirical method. Among the given states for the bilinear mode, four or more parameters are required to fully describe the behavior of the adherent region. In this article, due to the related state of the

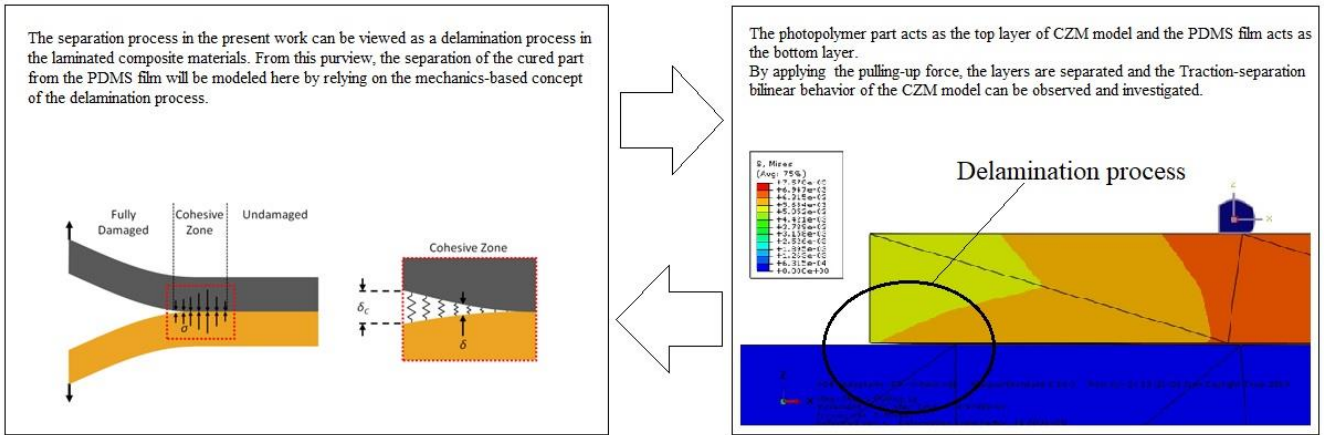


Fig. 10. Schema of the cohesive zone [3].

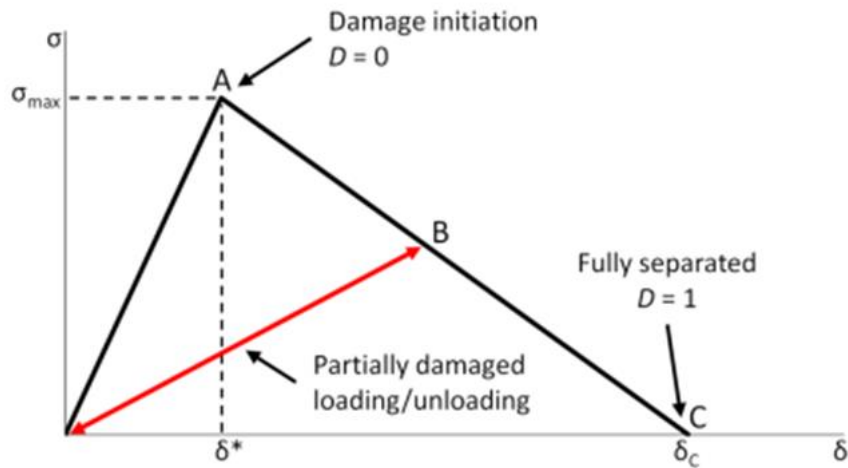


Fig. 11. Traction-separation bilinear behavior curve [3].

process and for simplifying the required parameters, a bilinear model is selected that can explain the structural behavior just with three parameters. In Fig. 11, at point A, damage begins at the critical stress value (σ_{max}). The separation phenomenon of the layers is computed with a damage parameter called D , as expressed in the following equation [3]:

$$D = \begin{cases} 0 & \text{if } \delta \leq \delta^* \\ \left(\frac{\delta - \delta^*}{\delta_c - \delta^*}\right) & \text{if } \delta^* < \delta < \delta_c \\ 1 & \text{if } \delta \geq \delta_c \end{cases} \quad (16)$$

As seen, when $\delta > \delta^*$, parameter D increases and when

$\delta > \delta_c$, parameter D reaches its maximum value, i.e. 1. Regardless of the δ value, the damage parameter D will never decrease. In other words, unloading will not reduce the amount of accumulated damage. Therefore, if the element of the cohesive region is initially loaded, for example in point B, it follows a trend that indicates a decrease in stiffness. By continuing the loading, the element will have the same stiffness reduction until it returns to point B, where the next damage begins. When $D = 1$, the element of the adhesive area is completely damaged and its stiffness tends to zero. At this moment, the damaged element is completely separated and will no longer interact with the layers.

In order to understand the theoretical principles of the separation process mechanism, finite element simulations are performed based on the concepts of stress analysis, so the process of pulling-up of solid part is fully considered based

on the displacement application and stress distribution on the surface.

This linear model assumes a linear elastic behavior at first and then the delamination process leads to damage propagation. The traction-separation law can be represented by the following matrix which relates the values of normal and shear stresses to normal and shear separations [3].

$$t = \begin{Bmatrix} t_n \\ t_s \\ t_t \end{Bmatrix} = \begin{bmatrix} K_{nn} & K_{ns} & K_{nt} \\ K_{ns} & K_{ss} & K_{st} \\ K_{nt} & K_{st} & K_{tt} \end{bmatrix} \begin{Bmatrix} \delta_n \\ \delta_s \\ \delta_t \end{Bmatrix} = k\delta \quad (17)$$

In this equation, K is the matrix of stiffness parameters, and t is the nominal traction vector, consisting of three components, which, in two-dimensional problems, becomes two components of t_n and t_s which represent respectively normal and shear stresses (in 3D modeling t_t is also available). The displacement motions for separation layers

are shown with δ_n , δ_s and δ_t . In the case of the current study, only the normal component is important, since the test samples only move in the vertical direction (normal to the plate). So it can be modeled here with the first loading mode.

4- 2- Cohesive zone parameters extraction

By determining the parameters of the traction-separation law for bilinear behavior in cohesive zone model, the graphical shape is achieved, because these parameters represent the important points of the related diagram. Generally, in order to specify a triangle on the coordinate plane, six independent parameters are needed, which are the horizontal and vertical coordinates of each vertices. For a triangular geometry representation for the linear behavior of an adhesive region model, one of the vertices is situated in the origin of coordinates. The vertical coordinate of the other vertex, which shows the separation occurrence, is put to zero, i.e. on abscissa. The other three coordinates need to be calculated. In this situation of the cohesive zone model, according to Fig. 15, it can be said that the vertical coordinates of point A , the slope of OA , and the area enclosed below the diagram are three parameters that are scientifically important and can be calculated. These three parameters represent the maximum nominal stress, stiffness and fracture energy, respectively. In the following, the method of calculating each of these parameters is discussed [14]. First, an initial guess is made for maximum nominal stress. It is expected that the amount of separation force obtained from the experimental test at a given moment is equal to the value of the stress integration underneath the studying cross-section, as:

$$F = \int_A T_n dA \quad (18)$$

where F is the traction force, A is the cross-section of the

sample part and T_n is the nominal normal stress. It is usual that the traction stress at a given moment does not have a uniform distribution at the desired surface. Therefore, in order to simplify the calculations and also to apply the most critical conditions in the process, the maximum force obtained in the experiment is calculated and thus, the maximum mean stress at the cross-section is considered as the initial guess for this value.

$$T^0 = T_{max}^{avg} = \frac{F_{max}}{A} \quad (19)$$

In this equation F_{max} is the maximum force measured directly via the experiment. The value of this parameter for each of the tests is shown in Table 2. In the second step, the stiffness parameter is investigated and according to the experiment, the amount of the maximum traction force has been measured. However, the separation measurement could not be carried out at that moment. On the other hand, the deformation of the silicon film and the photopolymer part is negligible compared to the separation distance. This approximation seems reasonable and valid in comparison with the amount of separation values. Based on this assumption, the rate of separation can be considered as a linear function of time in which velocity is considered constant. This can be illustrated as follows:

$$\delta = vt \quad (20)$$

Therefore, the stiffness parameter will be the result in dividing the maximum nominal stress by the separation rate:

$$K = \frac{T^0}{\delta^0} = \frac{T^0}{vt^0} \quad (21)$$

where t^0 is the time when the stress T^0 will arise and its value is obtained by experimental test. The value of this parameter for each one of the tests is given in Table 2.

The next step is to estimate the amount of fracture energy. The sum of the fracture energy ϵ can be obtained by calculating the area under the experimental force-separation curve:

$$\epsilon = \int_0^{\delta^f} F(\delta) d\delta \quad (22)$$

Here F is the traction force, δ is the separation value at the completion of the separation process (complete failure from the analysis of failure mechanics). The following relations will be obtained by substituting δ by vt :

Table 2. Calculated parameters required in the simulation for each test.

Test feature	$F_{max}(N)$	$T^0(MPa)$	$K(\frac{N}{mm^3})$	$\Gamma(\frac{N}{mm})$
A2	3.8235	0.33235	0.06643	0.113200
A3	5.8806	0.0261360	0.05220	0.113200
A4	17.4229	0.077430	0.10860	0.113200
P1	4.92	0.021860	0.054452	0.113200
P4	9.6785	0.043065	0.08603	0.113200
P9	14.6759	0.065226	0.130452	0.113200
V1=0.1mm/sec	3.0844	0.013708	0.001370	0.00541
V2=0.5mm/sec	5.8806	0.026136	0.110000	0.194733
V3=1.0mm/sec	14.852	0.064000	0.129616	1.16548
V4=3.0mm/sec	20.1467	0.089540	0.14923	7.9352
V5=5.0mm/sec	36.9917	0.164407	0.163444	39.3668

$$\varepsilon = \int_0^{\delta^f} F(\delta)d\delta = \int_0^{\delta^f} F(\delta)d(vt) = v \int_0^{t^f} F(t)dt \quad (23)$$

where t^f is the time of complete failure (point C in the diagrams). It can be seen from the above equation that for a given constant speed, the total fracture energy is equal to the integral of the traction force over time. The magnitude of the integral of the equation is equal to the area under the force-time curve at that velocity obtained by experimental testing for each one of the tests. Therefore, it can be said that the fracture energy of ε is nothing but a function of the area under the force-time diagram at its corresponding velocity. The approach investigated in this article evaluates how the contact cross-section in the cohesive area model and the fracture energy in this area are related to the cross-section geometry. Therefore, the correct failure energy will be obtained by dividing the total failure energy onto the area of the cross-section:

$$\Gamma = \frac{\varepsilon}{A} = \frac{v}{A} \int_0^{t^f} F(t)dt \quad (24)$$

The area under the force-time curves is easily calculated using the Quad function in Matlab® software. The lower limit of the integral is equal to zero and the upper limit is obtained by measurement in a practical experiment. The values of this parameter, like the other two parameters, are presented for

each test in Table 2.

4- 3- Finite element model

To model the process, numerical software of Abaqus® is used and two techniques are implied to model the behavior of the cohesive zone: Surface-based adhesion model and Adhesive-element model. Surface-based adhesion model is suitable for general state of traction-separation behavior with low adhesion layer thickness. On the other hand, adhesive elements model is used for the case where the thickness of the adhesive layer is considerable and its macroscopic properties are important.

Therefore based on the fact that the thickness of the adhesive layer is not estimated and the macroscopic properties in the process are not defined, the adhesive model based on the surface seems more appropriate. All the required parameters have been extracted from [14]. In the simulations, the behavior of both model components, i.e. the photopolymer part and the silicon film, are determined and their mechanical properties are chosen as follows:

Table 3. Mechanical properties of materials used in the process.

Material	Young's modulus (MPa)	Poisson's ratio
Photopolymer	2650	0.45
PDMS	0.36	0.49

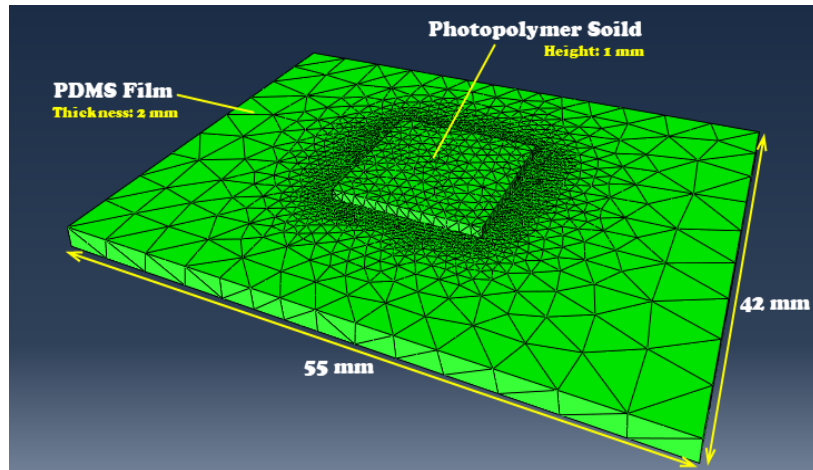


Fig. 12. The geometry is modeled on the actual dimensions in the process.

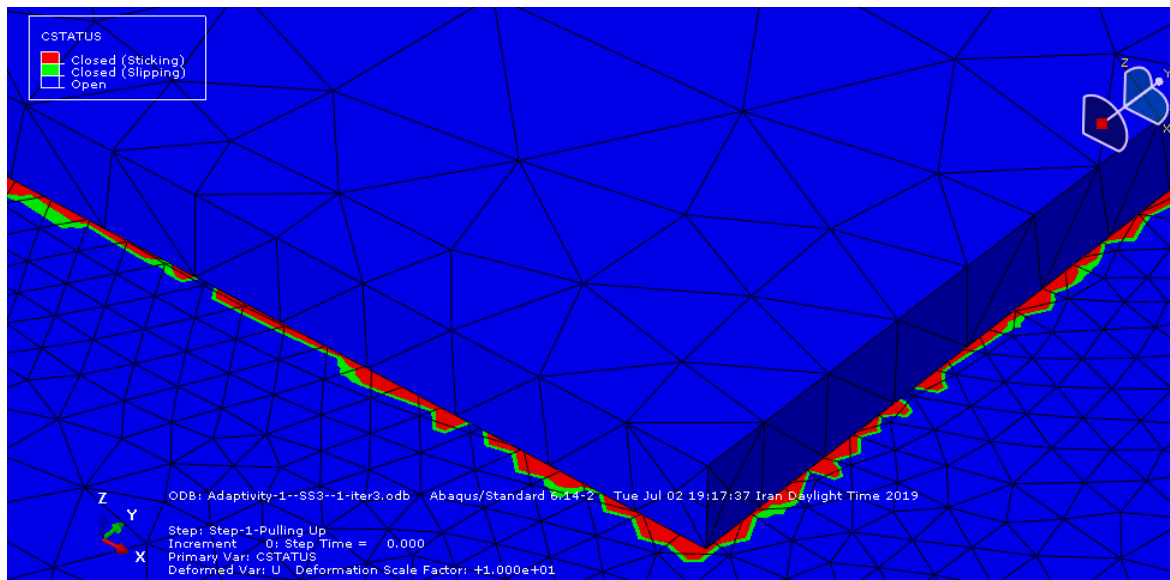


Fig. 13. Contact conditions during the separation process.

The film and part are meshed using C3D4 elements, which are tetrahedral elements with linear shape functions. The interface region on the film has a fine mesh and the remaining region has a coarse mesh. Since the part is rigid compared to film, it will undergo negligible deformations as compared to film and is meshed uniformly using a coarse mesh. An adaptive meshing technique has also been used for meshing of tetrahedron type elements for achieving sufficient accuracy in simulation. Adaptive meshing is an automated process that reduces computational cost by improving the quality of structural elements. The software first solves the model with the initial mesh determined by the user and then compares the result with the error index. If the error is not less than the specified value, it is meshes again and resolves the

model based on the calculations internally executed by the software, and continues until the error is less than the desired error value. The adaptive meshing process is based on model geometry, loading type and boundary conditions. Therefore, if the loading or boundary conditions change, even if the structural geometry remains constant, the process should be repeated.

5- Results and Discussion

In this section, the achieved results are given to evaluate the proximity of the experimental and FEM simulation results. The following diagrams are obtained from both experimental and analytical methods. As shown in Fig. 14, as the cross-section increases, the force required to separate the

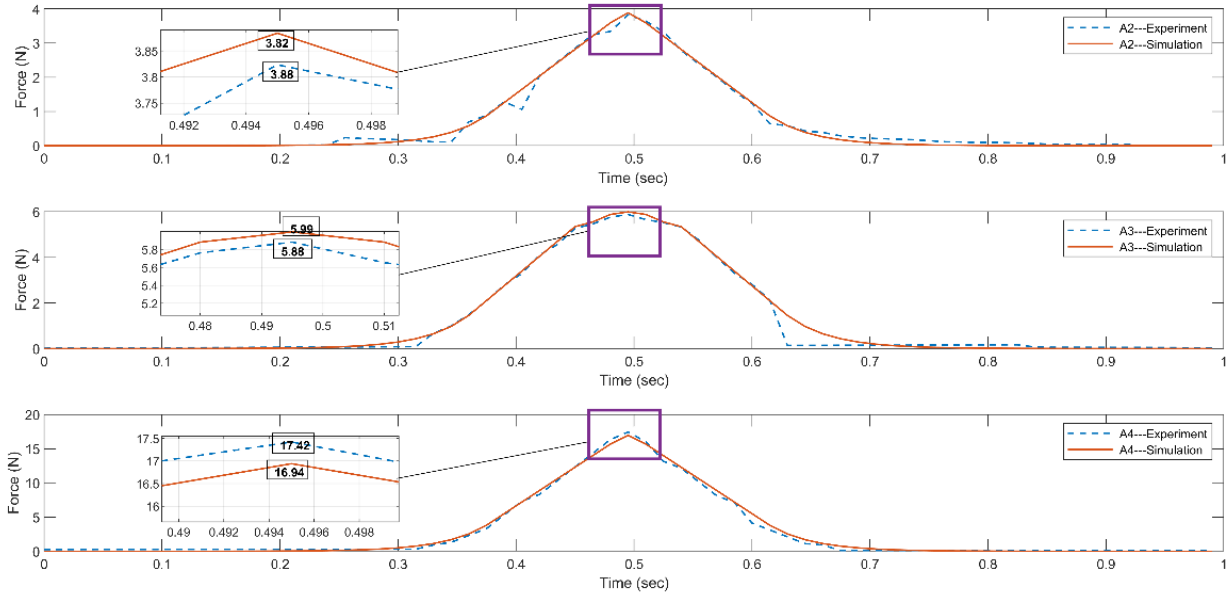


Fig. 14. Diagrams of the force changes versus cross sectional area.

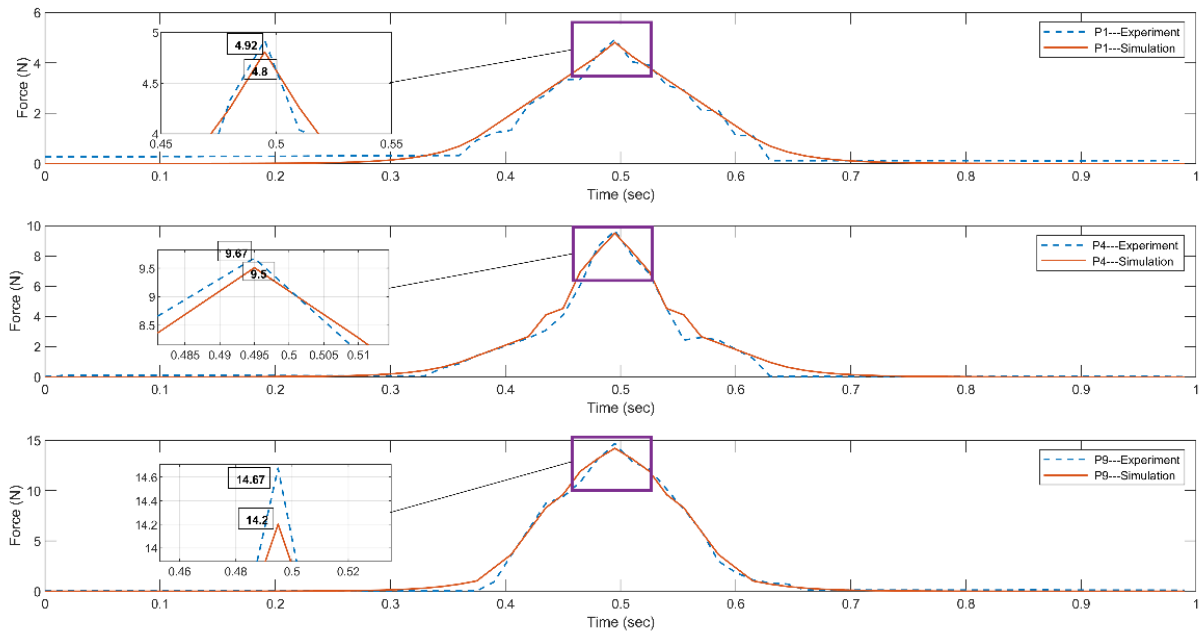


Fig. 15. Diagrams of the force changes against the geometry complexity.

layers from the bottom of the tank increases. The graphs also show that as the surface becomes larger, the force increases respectively. This problem is the biggest challenge facing large cross-section 3D printing.

Experiments have shown that the force increases with increase of the geometric complexity in part layers. On the

other hand, the A/L ratio is reduced. This decreasing ratio reinforces this hypothesis that the separation force should also be reduced. But the experiments show that the effect of the cross-section geometry is much greater than the one of the ratio. The mentioned results are shown in Fig. 15.

The most interesting part of the experiment concerns

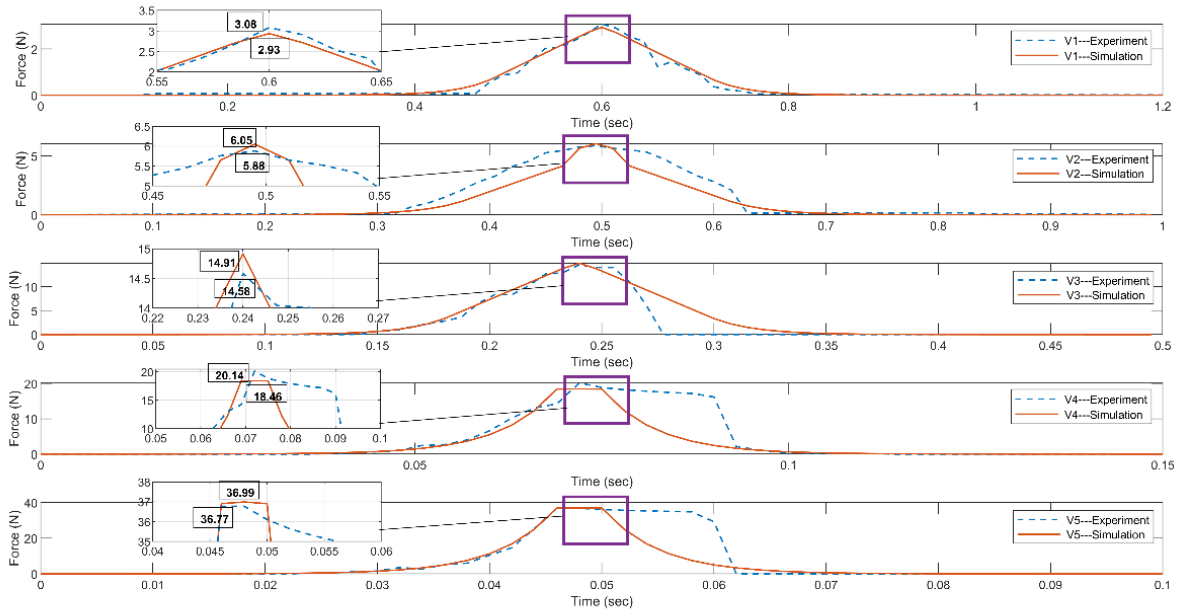


Fig. 16. Diagrams of the force variations versus motion velocity.

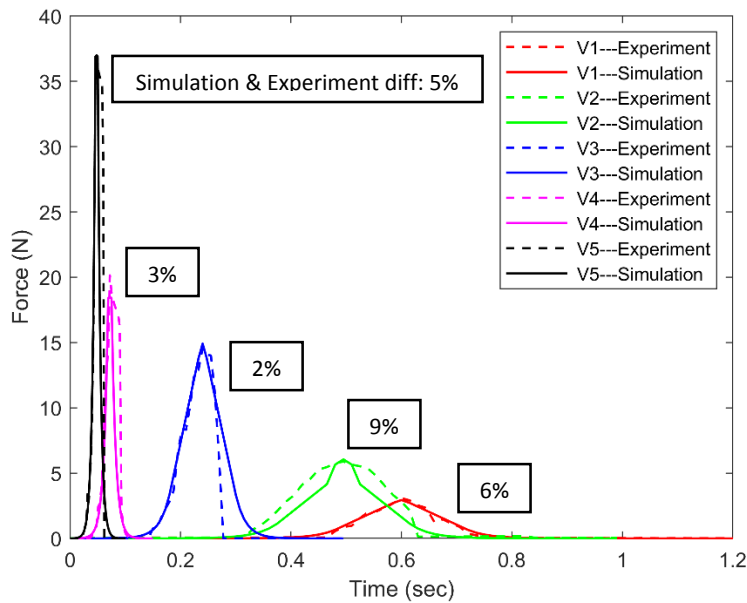


Fig. 17. Comparison of forces at different pulling-up velocities.

the effect of the platform speed. While the linear velocity increases, the difference between simulation and experimental results enlarges. This could be due to the impact of speed on dynamic behavior of the test setup. Whereas the simulation is performed in quasi-static conditions, the prediction error is aggravated. But the results are satisfactory in these conditions. The diagrams relating to this parameter are shown in Fig. 16. All of the five-velocity tests are measured on a single part and on different layers. By adding the initial height of the

process part during the simulation, it is tried to prepare the real conditions.

Also, the failure of the sampling parts happening at the application of maximum stress is simulated. As Fig. 18 indicates, an appropriate accuracy is achieved by the process simulation.

The last investigated subject is related to the process orientation of printing parts. Simulations have shown that edges with negative slope experience less stress than the

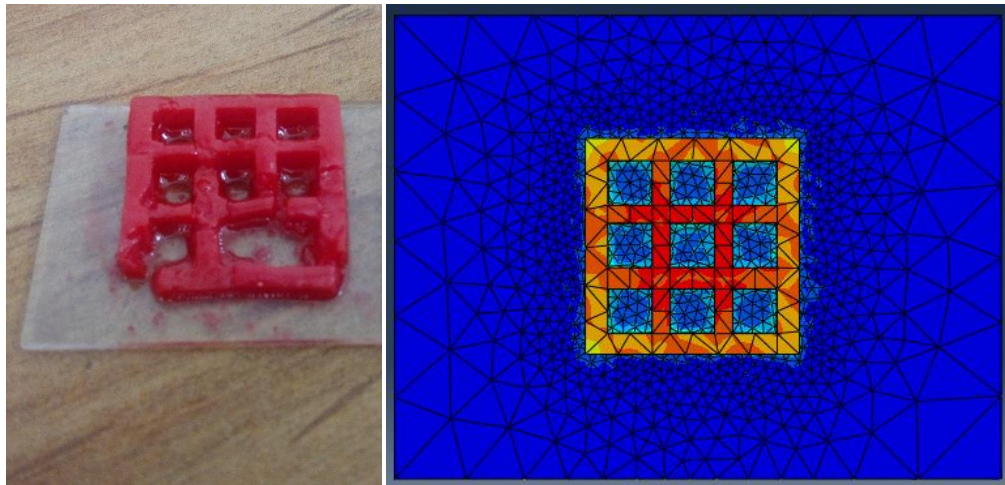


Fig. 18. Unsuccessful printing of the part and its failure due to the big separation forces.

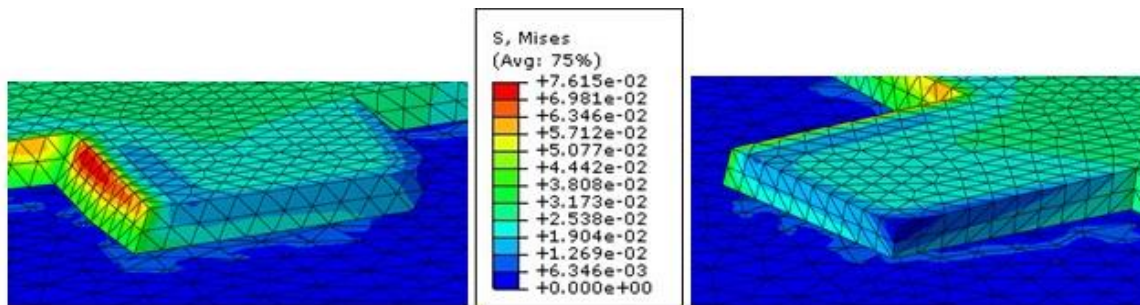


Fig. 19. Difference in stress distribution at positive or negative tips of sample parts.

edges with positive slope and are more vulnerable during the process. Fig. 19 shows the exactitude of this fact. It could be said that the larger area of contact zone in positive slope condition in comparison with the negative slope leads to larger surface attached to the process platform.

6- Conclusions

The cohesive zone model presented in this work is effective in predicting the separation force-time profiles resulting from the separation of the built-up part from the PDMS film. It is shown that the bilinear behavior of this fracture mechanics model is capable of predicting the maximum separation force. By comparing the experimental and simulation diagrams, it was seen that acceptable accordance between the maximum separation forces exists. However, this similarity was less respected during changes in force. One of the causes of this difference could

be the elastic deformation that occurs in the photopolymer part and the silicon film during the separation process and causes asymmetric stress distribution in the contact zone.

Another approach is the experimental tests condition; according to the results obtained from the velocity test, it is suggested that the simulation could be performed in dynamic mode, because based on the experimental test conditions; it is observed that when the process velocity increases, the difference between the experimental test and the simulation results are increased, and the generated error will be relatively high.

This study also showed that the process orientation of part should be considered at the design stage to prevent the large separation forces, which lead to the part failure. In other words, this design for manufacturing or DFM issues gives a handy tool to enlarge a printed part life cycle.

References

- [1] Technology Print me a Stradivarius How a new manufacturing technology will change the world. Retrieved March 18, 2020, from <http://www.economist.com/node/18114327>
- [2] B. Redwood, F. Schoffer, B. Garret, The 3D Printing Handbook, in: 3D Hubs B.V. Amsterdam, The Netherlands, (2017).
- [3] W.E.R. Krieger, Cohesive zone modeling for predicting interfacial delamination in microelectronic packaging, Thesis, Master of Science in the Woodruff School of Mechanical Engineering, Georgia Institute of Technology, (2014).
- [4] P.J. Bartolo, Stereolithography: Materials, Processes and Applications, Springer Pub, (2011).
- [5] H. Ye, A. Venketeswaran, S. Das, C. Zhou, Investigation of separation force for constrained surface stereolithography process from mechanics perspective, Rapid Prototyping Journal (2017).
- [6] J. Wang, S. Das, R. Rai, C. Zhou, Data-driven simulation for fast prediction of pull-up process in bottom-up stereo-lithography, Department of Mechanical and Aerospace Engineering, University at Buffalo (UB)-SUNY, United States, (2018).
- [7] SLA/DLP Basics By bad-zima in Workshop > 3D Printing. Retrieved December 03, 2019, from <https://www.instructables.com/id/SLADLP-Basics/>
- [8] Digital Light Synthesis™. Retrieved March 17, 2020, from <https://www.carbon3d.com/our-technology/>
- [9] X. Wu, Q. Lian, D. Li, Z. Jin, Tilting separation analysis of bottom-up mask projection stereolithography based on cohesive zone model, Journal of Materials Processing Technology, 243 (2017) 184–196.
- [10] F. Liravi, S. Das, C. Zhou, Separation force analysis and prediction based on cohesive element model for constrained-surface Stereolithography processes, Computer-Aided Design, 69 (2015) 134-142.
- [11] Y. Pan, H. He, J. Xu, A. Feinerman, Study of separation force in constrained surface projection stereolithography, Department of Mechanical and Industrial Engineering, University of Illinois at Chicgo, Chicago, Illinois, USA, (2017).
- [12] Effects of print window material on separation force of 3d printed objects in dlp sla printing processes, NewPro3D – Forcast Research & Development Corp., University of British Colombia, Laboratory Report, (2018).
- [13] J.R. Tumbleston, D. Shirvanyants, Nikita Ermoshkin, Continuous liquid interface production of 3D objects, Carbon3D Inc., Redwood City, CA 94063, USA. Department of Chemistry, University of North Carolina, Chapel Hill, NC, (2015).
- [14] H. Ye, S. Das, C. Zhou, Investigation of separation force for bottom-up stereolithography process from mechanics perspective, Proceedings of the ASME (2015), International Design Engineering Technical Conferences &, Computers and Information in Engineering Conference, IDETC/CIE 2015, Boston, Massachusetts, USA.
- [15] Y.M. Huang, C.P. Jiang, On-line force monitoring of platform ascending rapid prototyping system, in: Journal of Materials Processing Technology 159 (2005) 257–264.
- [16] Q. Liana, F. Yanga, H. Xina, D. Li, Oxygen-controlled bottom-up mask-projection stereolithography for ceramic 3D printing, in: Ceramics International, 43 (2017) 14956–14961.
- [17] N. Guo, M.C. Leu, Additive manufacturing: technology, applications and research needs, in: Frontiers of Mechanical Engineering, 8 (2013) 215–243.
- [18] Formlabs, SLA vs. DLP: Guide to Resin 3D Printers. Retrieved March 17, 2020, from <https://formlabs.com/blog/3d-printing-technology-comparison-sla-dlp/>
- [19] J.Y. Lee, W.S. Tan, J. An, C.K. Chua, C.Y. Tang, A.G. Fane, T.H. Chong, The potential to enhance membrane module design with 3D printing technology, in: Journal of Membrane Science, 499 (2016) 480-490.
- [20] R. Krueger, Virtual crack closure technique: History, approach and applications, in: Applied Mechanics Reviews, 57(2) (2004) 109-143.
- [21] A. Tn, C.G. Dávila, P.P. Camanho, J. Costa, An engineering solution for mesh size effects in the simulation of delamination using cohesive zone models, in: Engineering Fracture Mechanics, 74 (2007) 1665-1682.
- [22] D. Xie, A. Wass, Discrete cohesive zone model for mixed-mode fracture using finite element analysis, in: Engineering Fracture Mechanics, 73(13) (2006) 1783-1769.

HOW TO CITE THIS ARTICLE

F. Yadegari, R. Fesharakifard, F. Barazandeh, Numerical and experimental investigation of effective parameters on separation force in bottom-up stereolithography process, AUT J. Mech Eng., 5(3) (2021) 401-418.

DOI: 10.22060/ajme.2020.18408.5903



